Biophysics and Physicobiology

Regular Article

Confirmation of the formation of salt bridges in the denatured state of CutA1 protein using molecular dynamics simulations

Katsuhide Yutani[1], Yoshinori Matsuura[1] and Yasumasa Joti[1,2]

[1]*RIKEN SPring-8 Center, Sayo, Hyogo 679-5148, Japan*
[2]*Japan Synchrotron Radiation Research Institute, Sayo, Hyogo 679-5198 Japan*

It remains unclear how the abundant charged residues in proteins from hyperthermophiles contribute to the stabilization of proteins. Previously, based on molecular dynamics (MD) simulations, we proposed that these charged residues decrease the entropic effect by forming salt bridges in the denatured state under physiological conditions (Yutani *et al.*, *Sci. Rep.* **8**, 7613 (2018)). Because the quality of MD results is strongly dependent on the force fields used, in this study we performed the MD simulations using a different force field (AMBER99SB) along with the one we used before (Gromos43a1), at the same temperatures examined previously as well as at higher temperatures. In these experiments, we used the same ionic mutant (Ec0VV6) of CutA1 from *Escherichia coli* as in the previous study. In MD simulations at 300 K, Lys87 and Arg88 in the loop region of Ec0VV6 formed salt bridges with different favorable pairs in different force fields. Furthermore, the helical content and radius of gyration differed slightly between two force fields. However, at a higher temperature (600 K), the average numbers of salt bridges for the six substituted residues of Ec0VV6 were 0.87 per residue for Gromos43a1 and 0.88 for AMBER99SB in 400-ns MD simulation, indicating that the values were similar despite the use of different force fields. These observations suggest that the charged residues in Ec0VV6 can form a considerable number of salt bridges, even in the denatured state with drastic fluctuation at 600 K. These results corroborate our previous proposal.

Key words: hyperthermophile, protein stability, ion–ion interaction, charged residue, denatured sate of a protein

Proteins from hyperthermophiles, which have optimal growth temperatures near the boiling point of water, are much more stable than those from mesophilic organism, which grow at moderate temperatures near 37°C [1,2]. Hyperthermophile proteins have a high content of charged residues and are thought to be stabilized by ion–ion interactions, which permit the organisms to grow at high temperatures [3–12]. However, it remains unclear how the abundant charged residues contribute to the stabilization of hyperthermophile proteins. The CutA1 protein from the hyperthermophile, *Pyrococcus horikoshii*, (PhCutA1) has an unusually high denaturation temperature of nearly 150°C and an unusually high content of charged residues (42.2% of amino acid residues, vs. 22.3% for CutA1 from *Escherichia coli* (EcCutA1)) [13]. However, many charged residues in

◄ *Significance* ►

It remains unclear how the abundant charged residues in proteins from hyperthermophiles contribute to the stabilization of proteins. Previously, based on MD simulations, we proposed that the charged residues contribute to their conformational stabilities via entropic effects due to the formation of salt bridges in the denatured state, which equilibrates with the native state under physiological conditions. Because the quality of MD results is strongly dependent on the force fields used, in this study we performed the MD simulations using a different force field at more severe conditions. Obtained results corroborated our previous proposal.
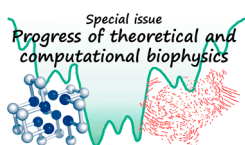
PhCutA1 do not exhibit favorable energies for ion–ion interactions [7].

Recently, to investigate this issue, we performed molecular dynamics (MD) simulation suggesting that ion–ion interactions in the denatured state stabilized hyperthermophile proteins [14]; the proposed mechanism is comparable to the stabilization conferred by intramolecular disulfide bonds. Disulfide bonds conformationally stabilize proteins by decreasing the entropy in the denatured state [15]. In our MD simulation, we used an SH-free mutant of EcCutA1 (Ec0SH) with a denaturation temperature (T_d) of 85.6°C, a hydrophobic mutant (Ec0VV) with T_d of 113.2°C, and an ionic mutant (Ec0VV6) with T_d of 136.8°C [16–18]. Ec0VV6 differs from Ec0VV by the addition of six charged residues, and has a T_d that is 23.6°C higher. In MD simulations, the average occupancy (proportion) of salt bridges by the six substituted charged residues of Ec0VV6 was 140.1% at 300 K, 84.3% at 400 K, and 89.5% at 450 K, indicating that even in the heat-denatured state, the proportion of salt bridges is 60.2% and 63.9% of the level observed at 300 K.

MD simulations are powerful tools for structural characterization of proteins, but the quality of the results is strongly dependent on the force field used [19–22]. Therefore, in order to confirm this observation (i.e., the formation of salt bridges in the denatured state), in this study we used two different force fields for MD simulations: Gromos43a1 [23] and AMBER99SB [24]. Gromos43a1, which was used in the previous paper, is a united-atom representation for aliphatic CH_n groups, whereas AMBER99SB is an all-atom representation. In addition, in this work we performed the MD simulations of Ec0VV6 for longer periods: 2000 ns at 450 K. To examine the formation of salt bridges under more severe conditions, we conducted our MD simulations for up to 400 ns at 550 K and 600 K using both force fields. The salt bridge content for each of the six targeted charged residues of Ec0VV6 in 300 K MD simulations, used as a reference, differed significantly between the two force fields. However, using AMBER99SB, the salt bridge occupancies at 450 K, 550 K, and 600 K were 53.0%, 68.5%, and 88.5%, similar to the results obtained with Gromos43a1. These results confirm our previous report [14] that charged residues in a protein can form salt bridges in the denatured state, contributing to stabilization by decreasing entropic effects.

Materials and Methods

We used a CutA1 mutant with three identical subunits from *Escherichia coli*, Ec0VV6 (Fig. 1), as a model protein. Ec0VV6 is an SH-free, hydrophobic, ionic mutant with a denaturation temperature of 136.8°C, 23.6°C higher than that of the SH-free and hydrophobic mutant [14]. The substitutions for the ionic mutant are as follows: A39D/S48K/H72K/S82K/Q87K/T88R.

MD simulations were performed using GROMACS software (ver. 4.5.5) [25,26]. The missing atoms in the coordi-
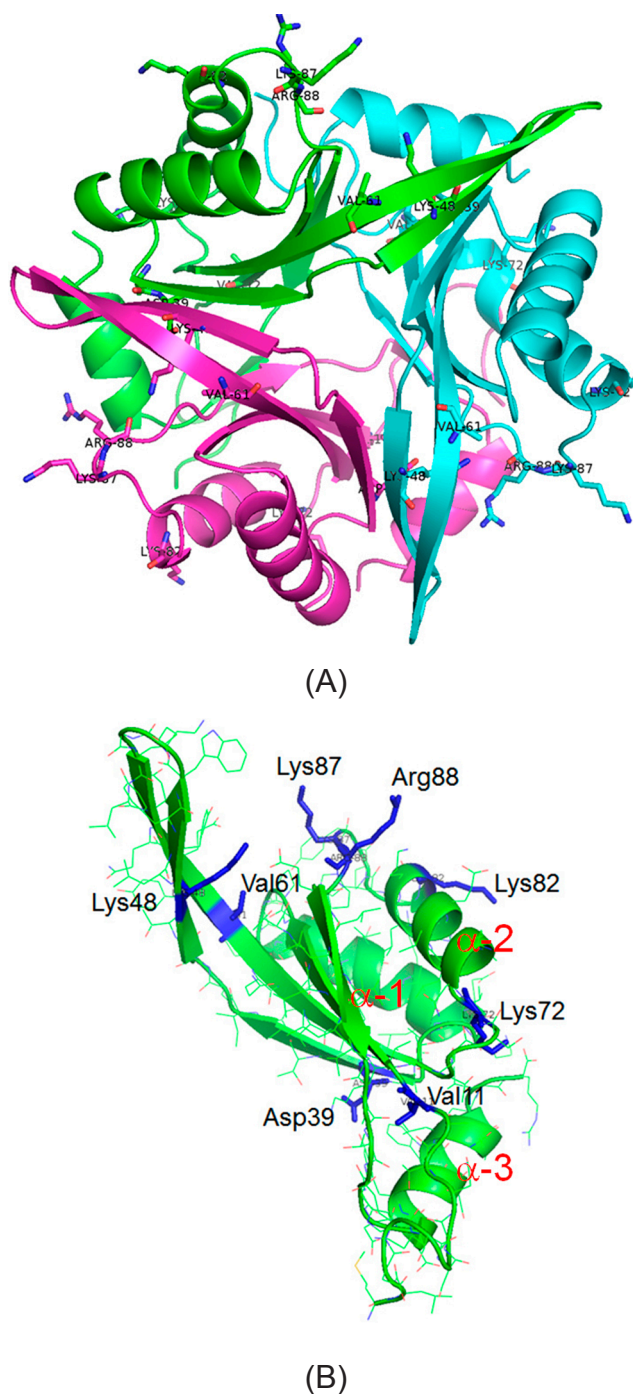

(A)

(B)

Figure 1 Tertiary structures of Ec0VV6 in MD simulations. (A) Native trimer structure of Ec0VV6 at 20 ns in the 300 K MD simulation (Gromos). Sticks represent targeted residues [14]. (B) Monomer structure (A subunit) of Ec0VV6 at 20 ns in the 300 K MD simulation (Gromos). Sticks represent targeted residues. Helices are numbered from the N-terminus: α-1, α-2, and α-3 [14].

nate file of SH-free CutA1 from *E. coli* (Ec0SH) (PDB ID, 4Y65), which are three N-terminal residues of the B subunit and eight N-terminal residues of the C subunit, were modeled in QUANTA2000 (Accelrys) using the coordinates of N-terminal residues of the A subunit as a reference. The

structure of Ec0VV6 was modeled using FoldX, based on the structure of Ec0SH. Hydrogen atoms were added to each protein. The models were solvated in water boxes with a minimum distance of 1.2 nm between the protein and the box. Counter-ions were added to the model to neutralize any net charge. The periodic boundary condition was adopted and the long-range electrostatic interactions were computed using the Particle-Mesh-Eward (PME) method [27]. The Gromos43a1 [23] or AMBER99SB [24] force field and SPC/E water model [28] were employed. The system was weakly coupled to a heat bath by velocity rescaling [29] with a relaxation time of 0.1 ps. A Parrinello–Rahman barostat [30] was used to maintain a pressure constant at 1 atm with a relaxation time of 0.5 ps. Hydrogen atoms were constrained using LINCS [31], and MD simulations at 300 K, 400 K, and 450 K were conducted with an integration time step of 1 femtosecond (fs). Energy minimizations were done to remove bad van der Waals contacts. Next, the temperature was raised from 50 K to 300 K in increments of 50 K, with 10,000 integration steps at each temperature and a harmonic constraint of C-alpha atoms. Thereafter, the ensemble was equilibrated through four 100-picosecond (ps) cycles with gradually released harmonic constraints: 1000, 100, 10, and 1 kJ mol^{-1} nm^{-2}. The subsequent MD stages for the EcCutA1 mutants were carried out without any restraint at 300 K. We also conducted the simulations at higher temperatures, 450 K, 550 K and 600 K. When the system temperature was increased to 450 K, 550 K or 600 K from 300 K, pressure coupling was not set for 1000 ps at 450 K, 550 K or 600 K. A Parrinello–Rahman barostat [30] was used to maintain a constant pressure of 6, 38, and 60 bar at 450 K, 550 K and 600 K, with a relaxation time of 0.5 ps, respectively.

The obtained MD trajectories were analyzed using the GROMACS software, as described previously [14]. However, for estimation of salt bridges, distance (using the command 'gmx distance') was calculated between C_ε atom of Lys (or C_ζ of Arg) and C_γ atom of Asp (or C_δ of Glu). We did not use 'gmx saltbr' as in the previous study because it did not function in the same way with the two force fields. Therefore, the occupancy of obtained salt bridges for which distance was less than 0.6 nm was slightly smaller in this study.

Results and Discussion

The crystal structure of EcCutA1 is a tightly intertwined trimer (Fig. 1A) very similar to that of PhCutA1, which has a denaturation temperature of nearly 150°C [13]. The stability of the Ec0VV6 mutant examined was about 50°C higher than that of wild-type EcCutA1, largely due to enrichment of hydrophobic and ionic interactions. We performed MD simulations at 450 K, 550 K, and 600 K for each monomer subunit of Ec0VV6 (Fig. 1B) using two different force fields, Gromos43a1 (hereafter, Gromos) and AMBER99SB (hereafter, Amber) to confirm the formation of salt bridges in the denatured state of Ec0VV6. As a reference, we performed 400-ns MD simulations at 300 K for the native trimer structure of Ec0VV6.

MD simulation of a trimer structure of Ec0VV6 at 300 K

Figures 2A and 2B show the trajectory of the root-mean-square deviations (RMSD) of all the C_α atoms from the crystal structure and the radius of gyration (Rg) for Ec0VV6, respectively, in 300 K MD simulations using different force fields. As shown in the figure, both values of RMSD have similar constant values after 140 ns. However, the Rg of the
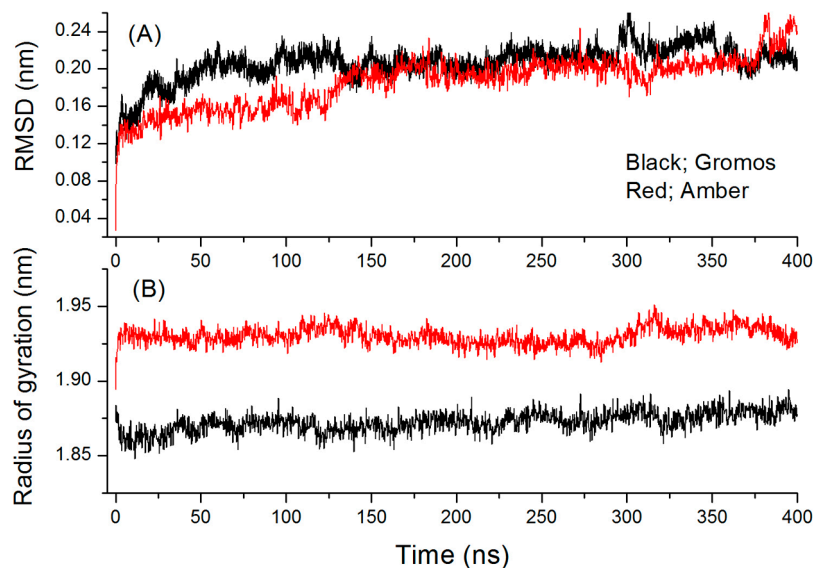

Figure 2   Trajectories of the RMSD (A) of C_α atoms and Rg (B) for the trimer of Ec0VV6 over 400 ns in the 300 K MD simulation. Black: Gromos; red: Amber.

Table 1 Comparison of RMSD and radius of gyration for Ec0VV6 with different force fields under the indicated conditions

	temp	interval (ns)	Gromos (nm)	Amber (nm)
RMSD	300 K	100–400	0.21 ± 0.01	0.20 ± 0.01
	450 K	1000–2000	1.52 ± 0.05	0.95 ± 0.05
	550 K	100–400	1.60 ± 0.08	1.80 ± 0.11
	600 K	100–400	1.70 ± 0.07	1.80 ± 0.10
Radius of gyration	300 K	100–400	1.87 ± 0.00	1.93 ± 0.01
	450 K	1000–2000	1.33 ± 0.02	1.47 ± 0.03
	550 K	100–400	1.41 ± 0.03	1.70 ± 0.11
	600 K	100–400	1.47 ± 0.04	1.69 ± 0.09

"±" represents the standard deviation from average values for three subunits during simulations

trimer structures changed in the opposite direction under the two different force fields; with Amber, the Rg of the protein increased, whereas with Gromos, it decreased (Table 1). The difference in Rg was 0.06 nm; this large difference between force fields was also observed in PhCutA1 at 300 K MD (manuscript in preparation). The average residue numbers of secondary structures in Ec0VV6 in 300 K MD simulations using the two force fields are listed in Table 2. The residue numbers of total secondary structures (including β-sheet, α-helix, β-bridge, and turn) were quite similar to each other, but the α-helix content was higher when using Gromos. The difference in helicity between the two force fields for each residue of Ec0VV6 was examined in a 300 K MD simulation (50–400 ns) (Supplementary Fig. S1). The three largest differences in helicity were 57.4% at Lys30, 49.3% at Lys82, and 56.9% at Ala109, which are near the C-terminal of the α-1, α-2, and α-3 helix, respectively (Fig. 1B). The increase in helicity using Gromos was also observed at Val70 (35.3%), which is near the N-terminal of α-2 helix. Yoda *et al.* [32] reported that for small peptides, Amber favors α-helix and Gromos favors β-hairpin.

It is important to determine the strength of salt bridges in a protein using MD simulations [33–36]. Hence, we examined the differences in formation of salt bridges for the additional six charged residues in Ec0VV6 in 300 K MD simulations using different force fields. Typical trajectories of distance between favorable charged residues in the Ec0VV6 trimer in 300 K MD simulations were shown in Supplemen-

tary Figure S2. Lys72 of Ec0VV6 can form a salt bridge with the C-terminal carboxyl group of Arg112 in the same subunit. The fluctuations of salt bridges between Lys72 and the C-terminal did not differ significantly among the three subunits, but the length of the salt bridge is slightly longer in the case of Amber (Supplementary Fig. S2A). The configurations of the salt bridge between Lys72 and the C-terminal of A subunit at 100 ns in 300 K MD simulations using the both force fields are shown in Supplementary Figure S3; the lengths of the salt bridge are 0.32 and 0.48 nm for Gromos and Amber, respectively. The salt bridges between Arg88 and Asp102 form an inter-subunit interaction at the initial state of Ec0VV6. The salt bridge seems to be very stable in 300 K MD simulations in the case of Amber, whereas they fluctuated drastically (Supplementary Fig. S2B) in the case of Gromos. The snapshots of Ec0VV6 at 100 ns show a large difference in the distance between Arg88 in the A subunit and Asp102 in the B subunit due to differences in the force field (Figs. 3A and 3B). Arg88 in Figure 3A is very distant from Asp102 in the other subunit, whereas Lys87 forms a salt bridge with Glu59 in the same subunit. On the other hand, when using Amber (Fig. 3B), Arg88 forms a strong salt bridge with Asp102 in the B subunit, whereas Lys87 is quite distant from Glu59 in the same subunit. Supplementary Figure S2C also shows that when using Gromos, but not Amber, Lys87 and Glu59 gradually formed salt bridges in MD simulations although the distance between them was quite large at the initial state. Arg88 was positioned near Asp102 in another subunit in the initial structure of Ec0VV6. However, because Arg88 moved farther from Asp102 in the other subunit in MD simulations when using Gromos, but not Amber, Lys87 also moved, resulting in formation of a salt bridge with Glu59 in the same subunit (Fig. 3A). The percent occupancies of ion pairs for substituted residues of Ec0VV6 when the distance of favorable ion pairs was less than 0.6 nm were calculated in 300 K MD simulations using the two different force fields (Supplementary Table S1). An occupancy value greater than 100% indicates that a charged residue forms more than one salt bridge. The average occupancy of six charged residues was 107.5% and 93.6% at 300 K for Gromos and Amber, respectively. These average values were quite similar to each other, but the difference at each charged residue was considerable; the occupancy of

Table 2 Comparison of residue number of secondary structures in Ec0VV6 in MD simulations using different force fields

Temperature	interval (ns)	Gromos			Amber		
		structure*	β-sheet	α-helix	structure*	β-sheet	α-helix
300 K	50–400	85.5 ± 1.6	42.9 ± 1.4	35.3 ± 0.9	85.1 ± 1.6	42.7 ± 1.4	32.6 ± 0.9
450 K	1000–1500	38.6 ± 4.6	19.6 ± 4.3	0.7 ± 1.1	68.6 ± 3.4	31.7 ± 2.2	21.4 ± 2.3
	1500–2000	39.7 ± 4.6	20.5 ± 4.2	0.5 ± 1.0	71.8 ± 3.8	33.2 ± 2.7	22.3 ± 2.4
550 K	100–400	27.2 ± 5.8	2.5 ± 3.0	0.4 ± 0.8	34.0 ± 6.6	1.6 ± 2.3	8.9 ± 4.9
600 K	100–400	23.7 ± 5.3	1.4 ± 2.0	0.4 ± 0.8	31.5 ± 6.5	0.9 ± 1.5	7.4 ± 4.5

* structure = β-sheet + α-helix + β-bridge + turn
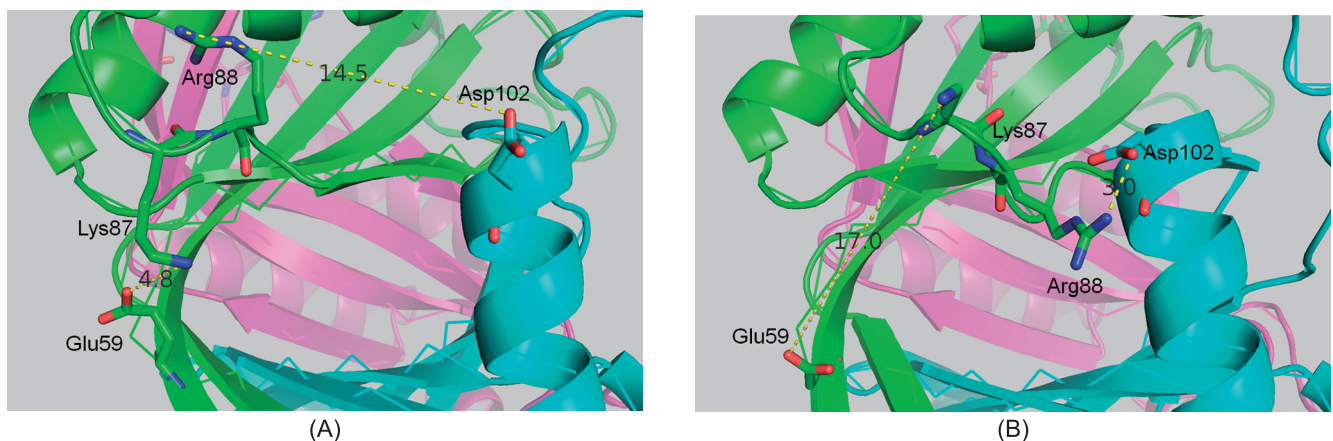Values represent the average number of secondary structures.

(A)   (B)

Figure 3 Configuration of different salt bridges for Lys87 and Arg88 in the loop region in 300 K MD simulations using both force fields. Green, blue, and magenta represent the A-, B-, and C-subunit, respectively. (A) Force field: Gromos. The distance between Lys87 and Glu59 in the A-subunit is 0.48 nm, whereas the distance between Arg88 in the A-subunit and Asp102 in the B-subunit is 1.45 nm. (B) Force field: Amber. The distance between Arg88 in the A-subunit and Asp102 in the B-subunit is 0.30 nm, whereas the distance between Lys87 and Glu59 in the A-subunit is 1.70 nm.

Lys87 was 60.3% and 1.4% at 300 K for Gromos and Amber, respectively (Supplementary Table S1). These results suggest that the formation of salt bridges in MD simulations differs significantly between force fields [33–36].

MD simulations of a monomer structure of Ec0VV6 at 450 K, 550 K, and 600 K

To confirm the formation of salt bridges of Ec0VV6 in the denatured state, we performed MD simulations for the monomer structures of Ec0VV6 at 450 K, 550 K, and 600 K using two different force fields. Because large differences between two force fields in the RMSD values of Ec0VV6 were detected at 450 K, the simulations were extended for longer periods (2000 ns vs. the previous value of 1400 ns).

However, as shown in Figure 4, the differences in RMSD value between the two force fields did not decrease in the 2000-ns simulations at 450 K. We did not detect large differences in RMSD at 550 K and 600 K, but the values for Amber were slightly greater and tended to fluctuate more (Table 1). The differences between the two force fields in Rg of the monomer Ec0VV6 at higher temperatures were greater than that of the trimer Ec0VV6 at 300 K (Table 1 and Supplementary Fig. S4). The Rg for monomers decreased due a change in structure, from ellipsoid (Fig. 1B) in the native trimer (Fig. 1A) to globular in the disordered monomer (Supplementary Fig. S5A). There were large differences in the secondary structures at 450 K between Gromos and Amber (Table 2); α-helical structures were completely
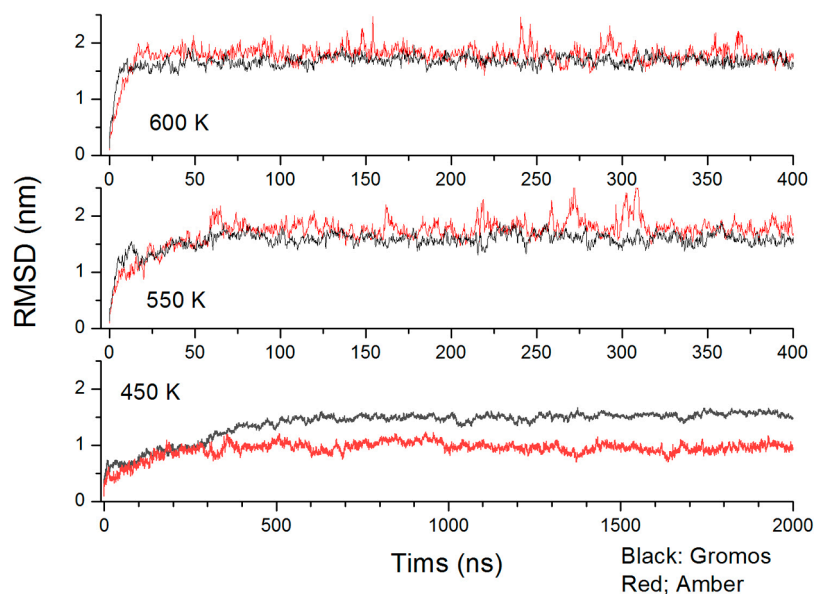

Figure 4 Trajectories of the RMSD of C_α atoms for the monomer of Ec0VV6 in MD simulations at 450 K, 550 K, and 600 K. Black and red represent data obtained with Gromos and Amber, respectively. Data represent the average values of three subunits.

destroyed at 450 K in the case of Gromos, but two-thirds of them were maintained in the case of Amber. These results are consistent with the large difference in RMSD data between the two force fields (Table 1).

The formation of salt bridges for six substituted residues of Ec0VV6 at high temperatures

A salt bridge is considered to form when the distance between favorable pairs of charged residues is less than

0.6 nm [36]. Because a considerable amount of salt bridges was detected even at 450 K, as reported previously [14], we performed MD simulations of Ec0VV6 at higher temperatures, 550 K and 600 K. In addition, we performed a simulation at 450 K using a different force field, Amber, at a longer period (up to 2000 ns). Figures 5A and 5B show typical trajectories of favorable ion–ion interactions at 450 K and 600 K, respectively. In the case of Gromos at 450 K (Fig. 5A), salt bridges between Arg88 and Asp20 that did not form
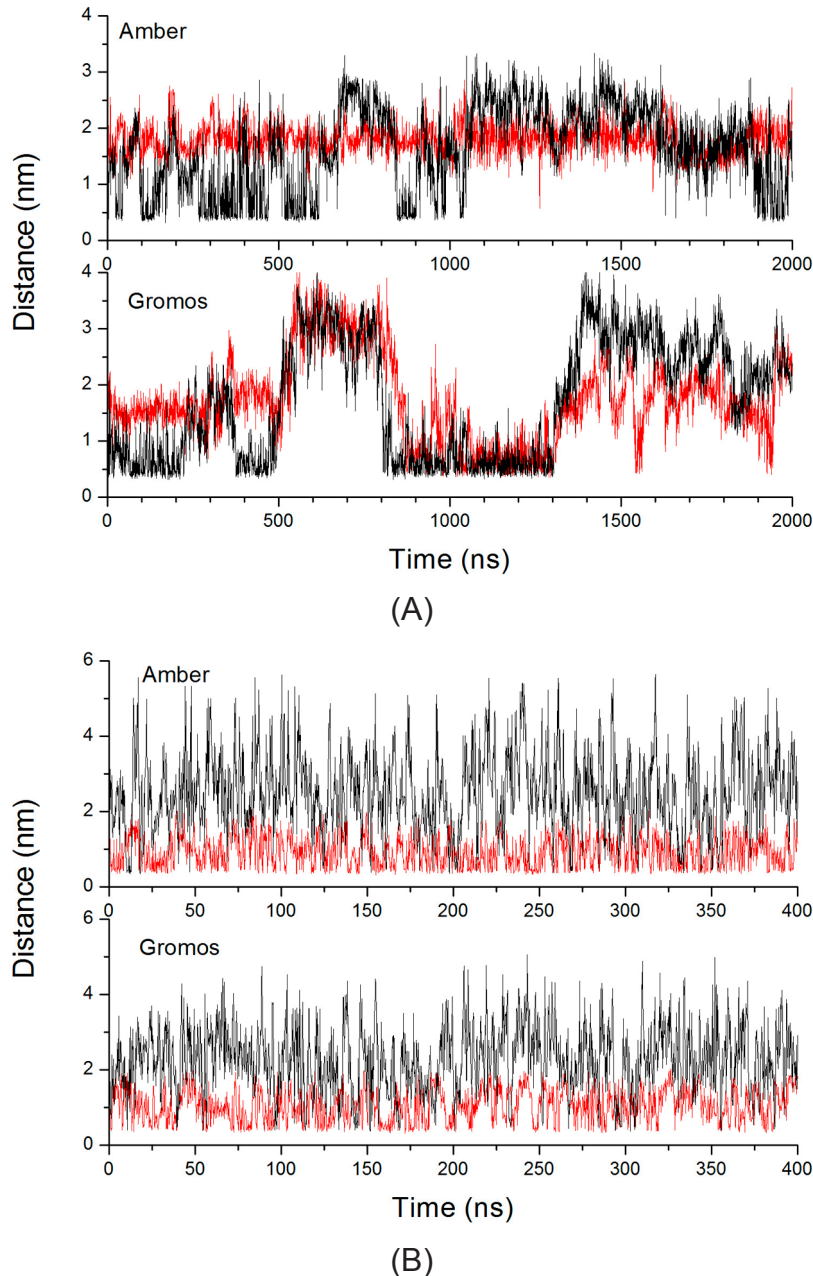

Figure 5 Trajectory of the length of typical salt bridges in the Ec0VV6 A-subunit at 450 K and 600 K. Upper and lower panels in each figure represent data obtained with Amber and Gromos, respectively. (A) Black and red represent the distances between the C_ε atom of Lys87 and the C_δ atom in Glu59, between the C_ζ atom of Arg88 and the C_γ atom of Asp20, respectively, in 450 K MD simulations performed over 2000 ns. (B) Black and red represent the distances between the C_ε atom of Lys72 and the C_δ atom of in Glu4, and between the C_ε atom of Lys82 and the C_δ atom of Glu78, respectively, in 600 K MD simulations performed over 400 ns.

at 300 K were detected in drastic fluctuations, whereas in the case of Amber, these fluctuations were suppressed, and consequently the salt bridges were not observed over the course of the 2000-ns simulation. These results are comparable with the increase in RMSD values and decrease in secondary structures observed with Gromos at 450 K. However, at 600 K (Fig. 5B), the fluctuation became more drastic, and the formation of salt bridges seemed not to differ between the two cases. Figure 5B indicates that Lys72 and Glu4, which are quite distant from one another in the primary sequence, can form salt bridges during drastic fluctuations, whereas Lys82 and Glu78, which are nearer to each other in the primary sequence, form salt bridges to a considerable degree even at the high temperature of 600 K.

Snapshots of salt bridges between Glu4 and Lys72 in 600 K MD simulations using different force fields are shown in Supplementary Figure S5. Strong salt bridges (0.29 nm) between these residues in Ec0VV6 were observed at 103 ns for Gromos (Supplementary Fig. S5A) and 18.2 ns for Amber (Supplementary Fig. S5B) in 600 K MD simulations. In the case of Amber, the α-helices were observed even at 600 K (Supplementary Fig. S5B, S5C), although no such secondary structures were observed in the case of Gromos (Supplementary Fig. S5A). In MD simulations using Amber, average number of residues forming an α-helix was 8.9 at 550 K and 7.4 at 600 K (Table 2). Glu4 and Lys72 of Ec0VV6 were quite distant from each other (5.03 nm) at 239 ns in 600 K MD simulations (Supplementary Fig. S5C), indicating the existence of an α-helix in a long ellipsoid.

All possible pair residues in Ec0VV6 are listed in Supplementary Table S1 (indicated by "pair residues") for each of six substituted residues. All percent occupancies shown in Supplementary Table S1 were greater than 1.0% at 550 K and 600 K for both force fields. This means that each of the six charged residues was able to form salt bridges with all the favorable ion pairs in Ec0VV6 in MD simulations at these temperatures.

Numbers of salt bridges for each of the six charged residues at high temperatures

The percent occupancies of favorable ion pairs with lengths below 0.6 nm for the six substituted residues of Ec0VV6 are listed in Supplementary Table S1. The values obtained with Gromos at 300 K and 450 K are consistent with reported ones [14] within experimental error, due to slight differences in the definition of distance between salt bridges and the period of MD simulations (see Materials and Methods). The average sum of the occupancies of six charged residues at 300 K was 107.5% in the case of Gromos, slightly higher than the value of 93.6% obtained with Amber. The sum of the occupancies for Lys87 and Arg88 at 300 K were 60.3% and 17.4%, respectively, in the case of Gromos, and 1.4% and 84.3% in the case of Amber (Supplementary Table S1). There were large differences between force fields in the occupancy at these two residues,

Table 3 Average number of salt bridges for six substituted residues of Ec0VV6 in MD simulations using different force fields

Temperatures	Force fields			
	Gromos		Amber	
	Number	Ratio*	Number	Ratio*
600 K	0.87 ± 0.16	0.80	0.88 ± 0.13	0.94
550 K	0.66 ± 0.10	0.61	0.69 ± 0.16	0.73
450 K	0.60 ± 0.10	0.55	0.53 ± 0.23	0.56
300 K	1.08 ± 0.85	1.00	0.94 ± 0.92	1.00

* Relative to the number of salt bridges at 300 K

which are located in a loop and move in different ways as described above (Figs. 3A and 3B). However, the average occupancies of ion pairs for the six charged residues at 550 K and 600 K were 66.1% and 86.7%, respectively, in the case of Gromos, and 68.5% and 88.5%, respectively, in the case of Amber (Supplementary Table S1), indicating that there were no significant differences between these two force fields. The occupancies were also higher than those obtained at 450 K using both force fields.

Table 3 shows the average numbers of salt bridges for each of six substituted residues of Ec0VV6 in MD simulations with different force fields. The values at 300 K were 1.08±0.85 for Gromos and 0.94±0.92 for Amber, indicating that the standard deviation is quite large. This is caused due to the fact that both Asp39 and Lys48 form salt bridge with two pairs, whereas Arg88 (Gromos) and Lys87 (Amber) barely engage in such interactions (Supplementary Table S1). On the other hand, the standard deviation at higher temperatures decreased considerably (Table 3). The values at 600 K were 0.87±0.16 for Gromos and 0.88±0.13 for Amber. Figure 6 shows the trajectories of average numbers for each salt bridge of the six substituted residues at 600 K. From the figure, it can be seen that about 90% of each charged residue formed constantly salt bridges with favorable pairs in 600 K MD simulation. These results indicate that the monomer structure of Ec0VV6 forms a considerable number of salt bridges, even in the denatured state, at temperatures of 550 K and 600 K.

Confirmation of the formation of salt bridges in the denatured state of Ec0VV6: Concluding remarks

Two different force fields, Gromos43a1 (a united-atom representation for aliphatic CH_n groups) and AMBER99SB (an all-atom representation) were used for MD simulations to confirm the formation of salt bridges in the denatured structures of CutA1 protein [14] at high temperatures. The stabilities of helical structures and Rg differed slightly between the two force fields in 300 K MD simulations; consequently, Lys87 and Arg88 in the loop region formed a salt bridge with different favorable pairs in the two force fields. However, at higher temperatures (550 K and 600 K), the specificity for favorable pair residues decreased, and each of the targeted charged residues constantly formed salt
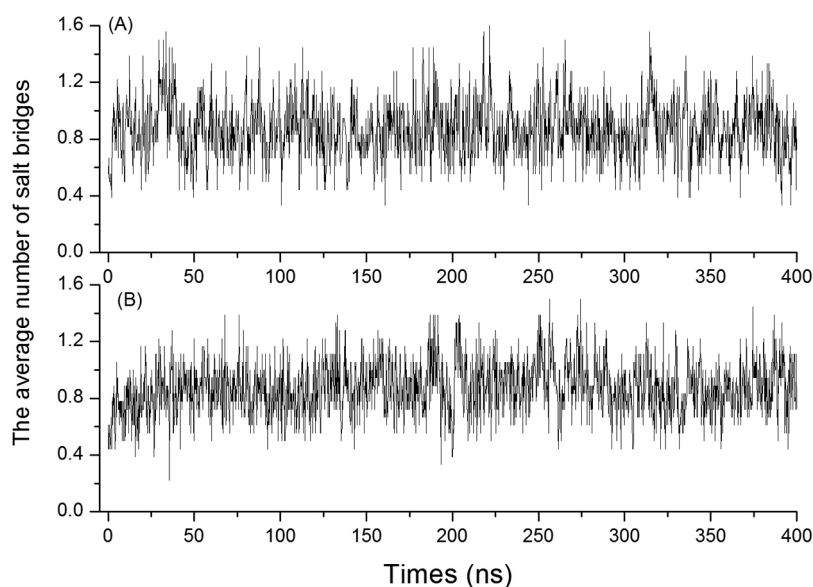
Figure 6 Trajectory of the average number of salt bridges per charged residue for six substituted residues in Ec0VV6 in 600 K MD simulations. (A) and (B) show data for Amber and Gromos, respectively.

bridges with a frequency of about 90% using both force fields. The ratio of formation of salt bridges at 600 K relative to 300 K was considerably high, 80% for Gromos and 94% for Amber (Table 3), indicating that charged residues in Ec0VV6 can form considerable amounts of salt bridges even in the denatured state, which is accompanied by drastic fluctuations. These results corroborate the findings of previous simulations performed at 400 K and 450 K. That is, the abundance of charged residues in proteins from hyperthermophiles might contribute to their conformational stabilities via entropic effects due to the formation of salt bridges in the denatured state, which equilibrates with the native state under physiological conditions.

Conflict of Interest

The authors declare no competing interests.

Author contributions

All authors designed the experiments, discussed the results, wrote the manuscript, and approved the final version for submission.

References

[1] Haney, P. J., Badger, J. H., Buldak, G. L., Reich, C. I., Woese, C. R. & Olsen, G. J. Thermal adaptation analyzed by comparison of protein sequences from mesophilic and extremely thermophilic Methanococcus species. *Proc. Natl. Acad. Sci. USA* **96**, 3578–3583 (1999).
[2] Suhre, K. & Claverie, J.-M. Genomic correlates of hyperthermostability, an update. *J. Biol. Chem.* **278**, 17198–17202 (2003).
[3] Ogasahara, K., Lapshina, E. A., Sakai, M., Izu, Y., Tsunasawa, S., Kato, I., *et al.* Electrostatic Stabilization in Methionine Aminopeptidase from Hyperthermophile, *Pyrococcus furiosus*. *Biochemistry* **37**, 5939–5946 (1998).
[4] Yamagata, Y., Ogasahara, K., Hioki, Y., Lee, S. J., Nakagawa, A., Nakamura, H., *et al.* Entropic stabilization of the tryptophan synthase α-subunit from a hyperthermophile, *Pyrococcus furiosus*. *J. Biol. Chem.* **276**, 11062–11071 (2001).
[5] Karshikoff, A. & Ladenstein, R. Ion pairs and the thermotolerance of proteins from hyperthermophiles: a "traffic rule" for hot roads. *Trends Biochem. Sci.* **26**, 550–557 (2001).
[6] Kaushik, J. K., Ogasahara, K. & Yutani, K. The unusually slow relaxation kinetics of the folding-unfolding of pyrrolidone carboxyl peptidase from a hyperthermophile, Pyrococcus furiosus. *J. Mol. Biol.* **316**, 991–1003 (2002).
[7] Matsuura, Y., Takehira, M., Sawano, M., Ogasahara, K., Tanaka, T., Yamamoto, H., *et al.* Role of charged residues in stabilization of Pyrococcus horikoshii CutA1, which has a denaturation temperature of nearly 150°C. *FEBS J.* **279**, 78–90 (2012).
[8] Sanchez-Ruiz, J. M. & Makhatadze, G. I. To charge or not to charge? *Trends Biotechnol.* **19**, 132–135 (2001).

[9] Sterner, R. & Liebl, W. Thermophilic adaptation of proteins. *Crit. Rev. Biochem. Mol. Biol.* **36**, 39–106 (2001).

[10] Vieille, C. & Zeikus, G. J. Hyperthermophilic enzymes: sources, uses, and molecular mechanisms for thermostability. *Microbiol. Mol. Biol. Rev.* **65**, 1–43 (2001).

[11] Guzman-Casado, M., Parody-Morreale, A., Robic, S., Marqusee, S. & Sanchez-Ruiz, J. M. Energetic evidence for formation of a pH-dependent hydrophobic cluster in the denatured state of *Thermus thermophilus* ribonuclease H. *J. Mol. Biol.* **329**, 731–743 (2003).

[12] Sadeghi, M., Naderi-Manesh, H., Zarrabi, M. & Ranjbar, B. Effective factors in thermostability of thermophilic proteins. *Biophys. Chem.* **119**, 256–270 (2006).

[13] Tanaka, T., Sawano, M., Ogasahara, K., Sakaguchi, Y., Bagautdinov, B., Katoh, E., *et al.* Hyper-thermostability of CutA1 protein, with a denaturation temperature of nearly 150°C. *FEBS Lett.* **580**, 4224–4230 (2006).

[14] Yutani, K., Matsuura, Y., Naitow, H. & Joti, Y. Ion–ion interactions in the denatured state contribute to the stabilization of CutA1 proteins. *Sci. Rep.* **8**, 7613 (2018).

[15] Pace, C. N., Grimsley, G. R., Thomson, J. A. & Barnett, B. J. Conformational stability and activity of ribonuclease T1 with zero, one, and two intact disulfide bonds. *J. Biol. Chem.* **263**, 11820–11825 (1988).

[16] Matsuura, Y., Ota, M., Tanaka, T., Takehira, M., Ogasahara, K., Bagautdinov, B., *et al.* Remarkable improvement in the heat stability of CutA1 from *Escherichia coli* by rational protein design. *J. Biochem.* **148**, 449–458 (2010).

[17] Matsuura, Y., Takehira, M., Joti, Y., Ogasahara, K., Tanaka, T., Ono, N., *et al.* Thermodynamics of protein denaturation at temperatures over 100°C: CutA1 mutant proteins substituted with hydrophobic and charged residues. *Sci. Rep.* **5**, 15545 (2015).

[18] Matsuura, Y., Takehira, M., Makhatadze, G. I., Joti, Y., Naitow, H., Kunishima, N., *et al.* Strategy for stabilization of CutA1 proteins due to ion-ion interactions at temperatures of over 100°C. *Biochemistry* **57**, 2649–2656 (2018).

[19] Piana, S., Donchev, A. G., Robustelli, P. & Shaw, D. E. Water dispersion interactions strongly influence simulated structural properties of disordered protein states. *J. Phys. Chem. B* **119**, 5113–5123 (2015).

[20] Sawle, L. & Ghosh, K. Convergence of molecular dynamics simulation of protein native states: Feasibility vs self-consistency dilemma. *J. Chem. Theory Comput.* **12**, 861–869 (2016).

[21] Riniker, S. Fixed-charge atomistic force fields for molecular dynamics simulations in the condensed phase: An overview. *J. Chem. Inf. Model.* **58**, 565–578 (2018).

[22] Robustelli, P., Piana, S. & Shaw, D. E. Developing a molecular dynamics force field for both folded and disordered protein states. *Proc. Natl. Acad. Sci. USA* **115**, E4758–E4766 (2018).

[23] Van Gunsteren, W. F., Billeter, S. R., Eising, A. A., Hunenberger, P. H., Kruger, P., Mark, A. E., *et al.* Biomolecular simulation: The GROMOS96 Mannual and User Guide; Vdf Hochshuverlag AG an der ETH Zurich: Zurich, Switzerland (1996).

[24] Hornak, V., Abel, R., Okur, A., Strockbine, B., Roitberg, A. & Simmerling, C. Comparison of multiple amber force fields and development of improved protein backbone parameters. *Proteins* **65**, 712–725 (2006).

[25] Hess, B., Kutzner, C., van der Spoel, D. & Lindahl, E. GROMACS 4: algorithms for highly efficient, load-balanced, and scalable molecular simulation. *J. Chem. Theory Comput.* **4**, 435–447 (2008).

[26] van der Spoel, D., Lindahl, E., Hess, B., van Buuren, A. R., Apol, E., Meulenhoff, P. J., *et al.* Gromacs User Manual version 4.5.4, www.gromacs.org (2010).

[27] Darden, T., York, D. & Pedersen, L. Particle mesh Ewald: An N-log (N) method for Ewald sums in large systems. *J. Chem. Phys.* **98**, 10089–10092 (1993).

[28] Berendsen, H. J. C., Grigera, J. R. & Straatsma, T. P. The missing term in effective pair potentials. *J. Phys. Chem.* **91**, 6269–6271 (1987).

[29] Bussi, G., Donadio, D. & Parrinello, M. Canonical sampling through velocity rescaling. *J. Chem. Phys.* **126**, 014101 (2007).

[30] Parrinello, M. & Rahman, A. Polymorphic transitions in single crystals: A new molecular dynamics method. *J. Appl. Phys.* **52**, 7182–7190 (1981).

[31] Hess, B., Bekker, H., Berendsen, H. J. C. & Fraaije, J. G. E. M. LINCS: A linear constraint solver for molecular simulations. *J. Comput. Chem.* **18**, 1463–1472 (1997).

[32] Yoda, T., Sugita, Y. & Okamoto, Y. Comparisons of force fields for proteins by generalized-ensemble simulations. *Chem. Phys. Lett.* **386**, 460–467 (2004).

[33] Debiec, K. T., Gronenborn, A. M. & Chong, L. T. Evaluating the strength of salt bridges: a comparison of current biomolecular force fields. *J. Phys. Chem. B.* **118**, 6561–6569 (2014).

[34] Zhou, X., Xi, W., Luo, Y., Cao, S. & Wei, G. Interactions of a water-soluble fullerene derivative with amyloid-β protofibrils: dynamics, binding mechanism, and the resulting salt-bridge disruption. *J. Phys. Chem. B.* **118**, 6733–6741 (2014).

[35] Ahmed, M. C., Papaleo, E. & Lindorff-Larsen, K. How well do force fields capture the strength of salt bridges in proteins? *Peer J* **6**, e4967 (2018).

[36] Thomas, A. S. & Elcock, A. H. Molecular simulations suggest protein salt bridges are uniquely suited to life at high temperatures. *J. Am. Chem. Soc.* **126**, 2208–2214 (2004).